Cite as:
Nguyen K, Camara A, Rio O, Sparowitz L (2017), Dynamic effects of turbulent crosswind on the serviceability state of vibrations of a slender arch bridge including wind-vehicle-bridge interaction. Journal of Bridge Engineering. Technical Note. 22(11): 06017005.

Dynamic effects of turbulent crosswind on the serviceability state of vibrations of a slender arch bridge including wind-vehicle-bridge interaction

K. Nguyen [1], A. Camara [2] O. Rio [3], L. Sparowitz [4]

ABSTRACT

The use of high performance materials in bridges is leading to structures that are more susceptible to wind- and traffic-induced vibrations due to the reduction in the weight and the increment of the slenderness in the deck. Bridges can experience considerable vibration due to both moving vehicles and wind actions that affect the comfort of the bridge users and the driving safety. This work explores the driving safety and comfort in a very slender arch bridge under turbulent wind and vehicle actions, as well as the comfort of pedestrians. A fully coupled wind-vehicle-bridge interaction model based on the direct integration the system of dynamics is developed. In this model, the turbulent crosswind is represented by means of aerodynamic forces acting on the vehicle

[1]Department of Continuum Mechanics and Structure Theories, School of Civil Engineering, Technical University of Madrid, Madrid, Spain. Email: khanh@mecanica.upm.es

[2]Department of Civil Engineering, School of Mathematics, Computer Science & Engineering, City University of London, UK. Email: Afredo.camara@city.ac.uk

[3]Former researcher of department of Construction, Eduardo Torroja Institute for Construction Science - CSIC, Serrano Galvache No 4, 28033, Madrid, Spain. Email: rio@ietcc.csic.es

[4]Laboratory for Structural Engineering, Graz University of Technology, Graz, Austria. Email:lutz.sparowitz@tugraz.at

and the bridge. The vehicle is modelled as a multibody system that interacts with the bridge by means of moving contacts that also simulate the road surface irregularities. An user element is presented with generality and implemented using a general-purpose finite element software package in order to incorporate the aeroelastic components of the wind forces, which allows to model and solve the wind-vehicle-bridge interaction in time domain without the need of using the modal superposition technique. An extensive computational analysis programme is performed on the basis of a wide range of the turbulent crosswind speeds. The results show that the bridge vibration is significantly affected by the crosswind in terms of the peak acceleration and the frequency content when the intensity crosswind is significant. The crosswind has more effect on the ride comfort of the vehicle in lateral direction, and consequently on its safety in terms of overturning accidents.

Keywords: turbulent wind, wind-vehicle-bridge-interaction, serviceability limit state of vibrations, human response to vibrations

INTRODUCTION

The concern about wind and traffic-induced vibrations of structures have increased in recent years. Road vehicles can be exposed to accident risks when crossing a location where the topographical features magnify the wind effects, such as bridges located in wind-prone regions. The recent advent of high-strength materials is leading to slender bridges that experience significant vibrations under moving vehicles and turbulent winds. Therefore, the comfort and safety of the bridge users (pedestrians and vehicle users) are important issues that cannot be neglected in the design of slender bridges. Recent studies in this field have been mainly focused on the driving comfort and safety of the vehicle running on the ground or in long span cable-supported bridges with conventional materials (Cai and Chen 2004; Xu and Guo 2004; Chen and Cai 2004; Guo and Xu 2006; Snæ björnsson et al. 2007; Sterling et al. 2010; Zhou and Chen 2015). Unfortunately, there is a clear lack of applications to other slender structures such as arch bridges. Furthermore, the comfort of other users of the bridge, such as pedestrians, has been routinely ignored.

In order to ensure the users' comfort, most codes and standards establish the design criteria for the Serviceability Limit State (SLS) of vibrations, in which two types of analysis procedures can be classified: deflection- and acceleration-based methods. The first one intends to control the bridge vibration by limiting the bridge deflection under a the static load. This is the approach followed by the American Association State Highway Transportation Officials (AASHTO) (American Association of State Highway and Transportation Officials 1998), which specifies a deflection criteria of L/800 for vehicular bridges and L/1000 for bridges with footpaths. Other criteria established in standards and guidelines (BS 5400-2:2006 2006; RPX-95 1995) uses a value calculated from the fundamental frequency of bridge. However, researchers and practitioners widely recognize that deflection limits are not appropriate for controlling the bridge vibrations (Wright and Walker 2004; Azizinamini et al. 2004; Roeder et al. 2004).

From the point of view of human comfort, the acceleration-based methods seem to be more rational because the human response depends on the characteristics of the excitation (Griffin 1990). Some codes (BS 5400-2:2006 2006; RPX-95 1995) propose a limit of the peak vertical acceleration $a_{lim} = 0.5\sqrt{f_0}$ (f_0 is the fundamental frequency of structure in Hz) for both footbridges and road bridges with footpath, but the use of this value is questionable. The acceleration of the deck nearby the abutments would far exceed the admissible limit when the vehicle enters and leaves the bridge (Moghimi and Ronagh 2008; Nguyen et al. 2015). This limit can also be easily exceeded anywhere on the deck if the pavement irregularities are large (Camara et al. 2014; Nguyen et al. 2015). Additionally, (Boggs and Petersen 1995) observed that the application of some laboratory test results based on the peak acceleration results in unrealistically severe evaluations in real buildings which are inconsistent with observation. The Root Mean Square (RMS) acceleration seems to be the most appropriate index in the context of the evaluation of human comfort. In fact, the ISO 2631 (ISO 2631-1:1997 1997) and the BS 6841:1987 (BS 6841:1987 2012) propose the use of weighted RMS acceleration in vibration evaluation. However, no specified limit of weighted RMS acceleration is defined in these codes in order to assess the comfort. Furthermore, the human response to vibration depends not only on the exposure time, magnitude and direction of excitation, human posture, but also on the frequency content of the vibration. In this sense, the frequency weighting curve is widely used to incorporate the frequency-related human perception to the comfort evaluation. Irwin (Irwin 1978) suggested base curves for acceptable human response to the vibration of a bridge for both vertical and lateral direction. On the other hand, the ISO 2631 (ISO 2631:1978 1978) defines three distinct limit curves for whole-body vibration for different levels of exposure time (see Fig. III): i) exposure limits (concerned with the preservation of health or safety), ii) fatigue-decreased proficiency boundary (concerned with the preservation of working efficiency) and iii) reduced comfort boundary (concerned with the preservation of comfort). The vibration levels below the base curves are regarded as comfortable and those above these curves are considered uncomfortable. In the present investigation, the Irwin's curves for vertical and lateral bridge vibration in storm conditions are selected as base curves to assess the pedestrians' comfort, while the fatigue-decreased proficiency boundaries for 1-min exposure time are used as the base curve for the ride comfort evaluation of vehicle users.

In the last decades, there have been many comprehensive studies based on frequency- and time-domain analyses to estimate the wind-induced buffeting response of bridges (Davenport 1962; Scanlan 1978; Miyata and Yamada 1990; Chen et al. 2000; Xu et al. 2000; Xu and Guo 2003; Cai and Chen 2004). Favoured by the linear and elastic response of the bridges, almost all the studies are based on the modal superposition technique. This requires advanced coding skills to solve the coupled dynamic wind-vehicle-bridge interaction, which is hindering its widespread application by engineering practitioners and researchers. With the advancement of Finite Element (FE) methods and computing technologies, a variety of FE software, such as Abaqus, Ansys or Nastran have been widely applied to various disciplines. These software packages combine a friendly graphical user interface and powerful computational capabilities. One of the main difficulties of using commercial FE programs for wind engineering studies is the definition of the aeroelastic effects due to the dependence with the instantaneous deformed configuration, which is not included in standard distribution packages.

This work develops a new type of element that can be applied with generality to any commercial software in order to represent the aeroelastic components of wind forces. The proposed fully coupled wind-vehicle-bridge interaction model allows the direct time-domain integration of the system of dynamics which can be used to consider nonlinear effects such as the loss of contact between the wheels and the pavement, among others. This model is applied in an extensive analysis programme to assess the driving safety and users' comfort in a very slender arch bridge made of Ultra-High Performance Fiber-Reinforced concrete, focusing on the users comfort subject to turbulent crosswind.

THE BRIDGE AND ITS PAVEMENT

The Wild Bridge (Sparowitz et al. 2011) is part of the new Eastern access of Völkermakt (Austria) and uses Ultra High Performance Fiber Reinforced Concrete (UHPFRC), which confers design a remarkable slenderness and light-weight. The arched structure is adopted due to the shape of the valley as shown in Figure

2. Detailed description of this bridge can be found in (Nguyen et al. 2015).

A three-dimensional finite element model of the Wild Bridge was developed in Abaqus (SIMULIA 2011). The deck, arches and piers were modelled by means of three-dimensional beam elements. Some auxiliary surface elements are introduced in the model to materialize the deck surface. These elements do not have inherent stiffness and mass and are constrained rigidly to the deck beam elements, therefore, these elements are only used for establishing the contact between the tire element and the deck surface and distribute the forces to the beam elements. Multi-point constraints were used to impose the kinematic relationship between the node of the pier and the corresponding node of the deck in order to model the fixed connection between both. The deck is connected to the abutments by four elastomeric bearings (EBs) of $350 \times 300 \times 126$ mm that allow vertical and horizontal displacements. Each EB was modelled by means of linear springs representing the vertical and horizontal stiffness, according to (CEN 2005a).

The mechanical properties of the materials employed in different parts of the bridge have been obtained from the modal updating of site measurements conducted in a precursor work (Nguyen et al. 2015). These are summarized in the Table 1, including its designation, adopted and updated value, respective unit and references. The frequencies of the first six modes of vibration of the bridge are listed in the Table 2.

In this study, we focus on the study of the wind effects on the vehicle-bridge vibration, however, the road surface always has some geometric imperfections. In order to take this into account in the vehicle-bridge interaction, a road surface roughness is defined. Appropriate road roughness profiles under the left and right wheels are generated so that there is an adequate coherence between them accepting the hypothesis of the isotropy of the road surface (Dodds and Robson 1973; Kamash and Robson 1978). The road roughness profile is generated as a zero-mean stationary Gaussian random process and can be generated as the sum of a series of harmonics:

$$r_1(x) = \sum_{i=1}^{N} \sqrt{2G(n_i)\Delta n}\cos(2\pi n_i x + \phi_i) \tag{1}$$

and the second parallel profile at distance $2b$ is defined by (Sayers 1988):

$$r_2(x) = \sum_{i=1}^{N}(\sqrt{2G(n_i)\Delta n}\cos(2\pi n_i x+\phi_i)+\sqrt{2(G(n_i)-G_x(n_i))\Delta n}\cos(2\pi n_i x+\theta_i)) \tag{2}$$

in which N is the number of discrete frequencies n_i in range $[n_{min}, n_{max}]$, Δn is the increment between successive frequencies, ϕ_i is the random phase angle uniformly distributed from 0 to 2π, θ_i is other random uniformly distributed phase angles. $G(n)$ and $G_x(n)$ are the one-sided direct and cross power spectral density (PSD) functions, respectively. In this work, the PSD value at a reference frequency of 0.1 cycle/m is defined as 64×10^{-3} m^3 that corresponds to the "good" quality of road surface. A range of frequency of interest from 0.01 to 10 cycle/m as recommended by ISO 8608:1995 (ISO 8608:1995 1995) were also considered in this work.

THE VEHICLE

The high-sided truck model shown in Fig. 3 is considered in this work as it combines large velocities and exposed areas to wind. This vehicle model is consistent a large number of previous works (Xu and Guo 2003; Chen and Cai 2004; Snæ björnsson et al. 2007; Sterling et al. 2010). The high-sided truck is modelled as a multibody system composed by individual rigid bodies (the vehicle body and two rigid bodies for each axle set). The vehicle body connects to the axle sets by means of the suspension system, which is modelled by linear spring-dashpot elements. The tires are considered as the linear spring-dashpot elements, in which the bottom node has a contact with the bridge surface. The vehicle body has five degrees of freedom (DOFs): vertical displacement z_c, lateral displacement y_c, rolling motion θ_x^c, pitching motion θ_y^c and yawing motion θ_z^c. Each rigid body in either the front axle set or rear axle set is assigned two DOFs: vertical displacement z_{ij} and lateral displacement $y_{i,j}$ (where $i = r,\ f$ is the index for rear and front axle, respectively and $j = 1, 2$ distinguish the right and left wheels respect to the driver). A constraint is applied to the two rigid bodies of each axle set in order to put a rigid connection between them. Altogether, the vehicle model has 11 DOFs. The geometry and mechanical properties of the high-sided vehicle are listed in Appendix I.

Only one vehicle is considered to be crossing the bridge in each analysis. The presence of multiple vehicles in the deck is a more realistic traffic scenario. However, previous research works have observed that the vibration induced by other vehicles does not change significantly the contact forces of individual vehicles (Zhou and Chen 2015).

TURBULENT CROSSWIND GENERATION

The turbulent crosswind is characterized by its stochastic properties: turbulence intensity, integral length scale, power spectral density function and coherence function. For a certain point at height z in space, the wind speed $U(x, y, z, t)$ is composed of three components:

$$U(x, y, z, t) = \begin{pmatrix} U + u(t) \\ v(t) \\ w(t) \end{pmatrix} \tag{3}$$

where U is the mean wind speed and $u(t)$, $v(t)$, $w(t)$ are the fluctuating components of the wind in the longitudinal, lateral and vertical directions, respectively. The mean wind speed depends on the height z, the terrain roughness and terrain orography. The mean speed is adopted by the following expression (CEN 2005b):

$$U = k_r \ln\left(\frac{z}{z_0}\right) c_o(z) U_b \tag{4}$$

with k_r the terrain factor, z_0 the roughness length, $c_o(z)$ orography factor taken as 1.0 and U_b the basic wind speed at 10 m above ground of terrain. The terrain category II is considered for this study, therefore, the value of k_r and z_0 are 0.19 and 0.05 m, respectively. It is noted that expression (4) ignores possible funnelling effects induced by the narrow shape of the valley where the considered bridge is located. This is deemed acceptable since the scope of the paper is to apply a FE-based wind-vehicle-bridge interaction model to a slender arch bridge, without losing generality in the results by adopting a wind-profile that is particular to an specific emplacement.

The generation of the turbulent wind speed time-histories in different points in space is carried out by applying the method proposed by Veers (Veers 1988), considering that these time-histories of wind speed are different but are not independent. In order to apply the aerodynamic forces of turbulent wind on the bridge and vehicle, the time histories of turbulent wind components in 53 points (see Fig. 4) are generated. For this generation of time histories, the value of the basic wind speed U_b is firstly proposed, and the mean wind speed at each point are then calculated according to its height. The main data of simulating conditions are adopted as follows:

- Integral length scale: $L_u = 100$ m, $L_v = 0.25L_u$ and $L_\omega = 0.10L_u$ (Strømmen 2006)

- Turbulent intensities: $I_u(z) = 1/\ln(z/z_0)$, $I_v = 0.75I_u$ and $I_\omega = 0.50I_u$

(Strømmen 2006)

- Upper cutoff frequency: $f_{up} = 12.0$ Hz
- Dividing number of frequency: $N_f = 1024$
- Time interval: $dt = 0.002$ s

A range of the basic wind velocity from 5.0 to 30.0 m/s in increments of 0.5 m/s has been considered to study the influence of the crosswind velocity, Figure 4(b) shows the time histories of the longitudinal component of turbulent crosswind velocity at the two points indicated in figure 4(a) for $U_b = 10.0$ m/s.

WIND-VEHICLE-BRIDGE INTERACTION

The coupled vehicle-bridge system under turbulent crosswind is governed by a complicated dynamic interaction problem that involves interaction between the wind and the vehicle, the wind and the bridge, and the vehicle and the bridge. The interaction wind-vehicle and wind-bridge interaction is modelled through the aerodynamic forces applied to the vehicle and the bridge. A detailed description on how to obtain these aerodynamic forces is given in the next section. On the other hand, the vehicle-bridge interaction is established between the tires and the deck surface. In this study, a perfectly guided path is considered for the tire-deck surface interaction model, i.e. contact points between the tires and the deck surface share the position and velocity. In order to develop this tire-deck interaction model in Abaqus, a "node to surface" contact formulation (SIMULIA 2011) is used between the bottom node of the tire elements and the deck surface. The augmented Lagrange method is applied then for the kinematic relations to enforce the corresponding contact constraints. Using augmented Lagrange formulation, the force vector applied on the vehicle and the bridge systems due to the interaction can be determined as:

$$\begin{Bmatrix} \mathbf{F}_v^C \\ \mathbf{F}_b^C \end{Bmatrix} = \nabla \mathbf{\Phi}^T \mathbf{\Lambda} + \nabla \mathbf{\Phi}^T \mathbf{\Upsilon} \mathbf{\Phi} \tag{5}$$

where $\nabla \mathbf{\Phi}^T = \partial \mathbf{\Phi} / \partial \mathbf{x}$; $\mathbf{x} = [\mathbf{x}^v, \mathbf{x}^b]$ is the global vector of displacement unknowns, $\mathbf{\Phi}$ is the constraints vector that links the bottom node of the tire elements with the deck surface; $\mathbf{\Lambda}$ and $\mathbf{\Upsilon}$ are the Lagrange multiplier vector and the penalty matrix of the coupled system, respectively; $\mathbf{F}_v^c$ is force vector applied on the vehicle as consequence of the interaction with structure, and $\mathbf{F}_b^C$ their counterparts on the structure.

The proposed methodology is developed in Abaqus (SIMULIA 2011), which allows to model the bridge structure by means of finite elements and the vehicle using multibody systems. The multibody dynamic equilibrium equations include second order and nonlinear terms related to the inertial forces (gyroscopic, coriolis, centrifugal) that, in addition to the inherent nonlinearity introduced by the moving contact in the wheels, leads to a nonlinear coupled system of equations that defines the wind-vehicle-bridge interaction problem. This system can be expressed in the following matrix form, including the interaction forces and aerodynamic forces:

$$\begin{bmatrix} \mathbf{M}_v & \mathbf{0} \\ \mathbf{0} & \mathbf{M}_b \end{bmatrix} \begin{Bmatrix} \ddot{\mathbf{x}}_v \\ \ddot{\mathbf{x}}_b \end{Bmatrix} + \begin{bmatrix} \mathbf{C}_v & \mathbf{0} \\ \mathbf{0} & \mathbf{C}_b \end{bmatrix} \begin{Bmatrix} \dot{\mathbf{x}}_v \\ \dot{\mathbf{x}}_b \end{Bmatrix} + \begin{bmatrix} \mathbf{K}_v & \mathbf{0} \\ \mathbf{0} & \mathbf{K}_b \end{bmatrix} \begin{Bmatrix} \mathbf{x}_v \\ \mathbf{x}_b \end{Bmatrix} = \begin{Bmatrix} \mathbf{F}_v^w \\ \mathbf{F}_b^w \end{Bmatrix} + \begin{Bmatrix} \mathbf{F}_v^C \\ \mathbf{F}_b^C \end{Bmatrix} \tag{6}$$

where $\mathbf{F}_v^w$, $\mathbf{F}_b^w$ is the aerodynamic wind force vector applied on the vehicle and bridge, respectively; $\mathbf{M}_v$, $\mathbf{C}_v$, $\mathbf{K}_v$ are the mass, damping and stiffness matrix of the vehicle, respectively; $\mathbf{M}_b$, $\mathbf{C}_b$, $\mathbf{K}_b$ are the mass, damping and stiffness matrix of the bridge, respectively.

The HHT-α implicit integration method (Hilber et al. 1977) is used to solve the system of differential equations (6) in the time domain. A constant time step of 0.001 s is adopted, which is small enough to accurately capture high frequency vibrations and to account for the contribution of high-order spatial frequencies of the roughness profile.

WIND-INDUCED EFFECTS

Wind forces on the vehicle

The aerodynamics forces and moments acting on the running vehicle under crosswind are represented in Fig. 5. These are determined using the quasi-static approach according to (Snæ björnsson et al. 2007). Assuming that the mean wind velocity U is perpendicular to the longitudinal axis of the bridge deck (the x axis) and the vehicle runs over the bridge with a constant speed V the relative wind velocity U_R and the angle of incidence α (see Fig. 5) can be determined at each instant t as follows:

$$U_R(t) = \sqrt{(U + u(t))^2 + (v(t) + V)^2} \tag{7}$$

$$\alpha(t) = \arctan\left(\frac{U + u(t)}{v(t) + V}\right) \tag{8}$$

where $u(t)$ and $v(t)$ are the longitudinal and horizontal components of turbulent crosswind, respectively. It should be noted that the wind time-history applied on the running vehicle is different from that applied on the surrounding nodes of the deck, from which it is linearly interpolated maintaining the compatibility.

Wind forces on the bridge

Based on the buffeting theory, the wind induced forces on the bridge structure can be determined from the instantaneous velocity pressure and the loads coefficients. The wind-induced forces per unit length on the bridge may be expressed in vector form as follows (Strømmen 2006):

$$\begin{bmatrix} F_D(x,t) \\ F_L(x,t) \\ M_x(x,t) \end{bmatrix} = \frac{1}{2}\rho U_R^2 \begin{bmatrix} DC_D(\alpha_e) \\ BC_L(\alpha_e) \\ B^2 C_M(\alpha_e) \end{bmatrix} \tag{9}$$

where U_R is the instantaneous relative wind velocity, $C_D(\alpha_e),\ C_L(\alpha_e),\ C_M(\alpha_e)$ are drag, lift and moment aerodynamic coefficients that are functions of the angle of wind incidence α_e (see Fig. 6), D and B are height and width of deck bridge section. In structural axis, the equation (9) is transformed into:

$$\mathbf{F}_b^w(x,t) = \begin{bmatrix} F_y \\ F_z \\ M_x \end{bmatrix} = \begin{bmatrix} \cos\beta & -\sin\beta & 0 \\ \sin\beta & \cos\beta & 0 \\ 0 & 0 & 1 \end{bmatrix} \begin{bmatrix} F_D \\ F_L \\ M_x \end{bmatrix} \tag{10}$$

The formulation using the Scalan's frequency dependent flutter derivatives (Scanlan and Tomko 1971) is usually used in the modal frequency domain. However, in this study the dynamic calculation is performed in the direct time domain, therefore, the aerodynamic forces can be decomposed, using the linearization approach, as follows (Strømmen 2006):

$$\mathbf{F}_b^w = \underbrace{\mathbf{F}_s}_{\text{static}} + \underbrace{\mathbf{B}\cdot\mathbf{v}}_{\text{aerodynamic}} + \underbrace{\mathbf{C}_{ae}\cdot\dot{\mathbf{r}} + \mathbf{K}_{ae}\cdot\mathbf{r}}_{\text{aeroelastic}} \tag{11}$$

where $\mathbf{F}_s$, $\mathbf{B}\cdot\mathbf{v}$ and $\mathbf{C}_{ae}\cdot\dot{\mathbf{r}}+\mathbf{K}_{ae}\cdot\mathbf{r}$ represent the static, aerodynamic and aeroelastic effects, respectively, and are defined as:

$$\mathbf{F}_s = \frac{1}{2}\rho U^2 B \left.\begin{bmatrix} (D/B)C_D \\ C_L \\ BC_M \end{bmatrix}\right|_{\alpha_s} \tag{12a}$$

$$\mathbf{B} = \frac{1}{2}\rho U B \left.\begin{bmatrix} 2(D/B)C_D & (D/B)C'_D - C_L \\ 2C_L & C'_L + (D/B)C_D \\ 2BC_M & BC'_M \end{bmatrix}\right|_{\alpha_s} \tag{12b}$$

$$\mathbf{C}_{ae} = -\frac{1}{2}\rho U B \left.\begin{bmatrix} 2(D/B)C_D & (D/B)C'_D - C_L & 0 \\ 2C_L & C'_L + (D/B)C_D & 0 \\ 2BC_M & BC'_M & 0 \end{bmatrix}\right|_{\alpha_s} \tag{12c}$$

$$\mathbf{K}_{ae} = \frac{1}{2}\rho U^2 B \left.\begin{bmatrix} 0 & 0 & (D/B)C'_D \\ 0 & 0 & C'_l \\ 0 & 0 & BC'_M \end{bmatrix}\right|_{\alpha_s} \tag{12d}$$

$$\mathbf{v} = \begin{bmatrix} u & w \end{bmatrix}^T \tag{12e}$$

$$\mathbf{r} = \begin{bmatrix} p & h & \alpha \end{bmatrix}^T \tag{12f}$$

in which α_s is the angle of attack of the wind respect to the position of the bridge elements (deck, arch, piers) at the static equilibrium position. $p,\ h,\ \alpha$ are the horizontal, vertical and torsional displacement of the structure under turbulent wind (see Fig. 6). The prime symbol in $C'_D,\ C'_L,\ C'_M$ indicates derivation of the aerodynamic coefficients with respect to the angle of attack. These derivatives are obtained from the computational fluid dynamic analysis of the deck, arch and piers (see Appendix III). It can be seen that the static and aerodynamic parts are functions of the mean wind (U) and its turbulence (u and w), while the aeroelastic part is associated with the structural velocity and displacement. The static and aerodynamic parts can be introduced into the structural elements via nodal forces in Abaqus software. However, due to the structural motion dependence of the aeroelastic part there is no direct way to introduce these forces in Abaqus software. In order to model the aeroelastic wind forces an user element has been developed within Abaqus using user subroutine UEL (SIMULIA 2011). The basic idea used here is that the user element is attached to each node of the structural bridge element as shown in Fig. 7. The user element will provide to the model during the transient analysis steps the forces $\mathbf{F}_i$ at the node i that depend on the values of the degrees of freedom $\mathbf{X}_i^b$ at this node (each structural bridge element has six degrees of freedom).

It is noted that the forces $\mathbf{F}_i$ generated by user element must be the same aeroelastic wind forces acting on this node, therefore, the nodal forces $\mathbf{F}_i$ can be expressed as

$$\mathbf{F}_i = \mathbf{C}_i^{ae}\dot{\mathbf{X}}_i^b + \mathbf{K}_i^{ae}\mathbf{X}_i^b \tag{13}$$

where $\mathbf{K}_i^{ae}$ and $\mathbf{C}_i^{ae}$ represent the local aeroelastic stiffness and damping matrices at the node i, respectively. From the equations (12d) and (12e), the expressions of $\mathbf{K}_i^{ae}$ and $\mathbf{C}_i^{ae}$ can be determined as following

$$\mathbf{K}_i^{ae} = \frac{1}{2}\rho U^2 B l_{wi} \left.\begin{bmatrix} 0 & 0 & 0 & 0 & 0 & 0 \\ 0 & 0 & 0 & (D/B)C_D' & 0 & 0 \\ 0 & 0 & 0 & C_L' & 0 & 0 \\ 0 & 0 & 0 & BC_M' & 0 & 0 \\ 0 & 0 & 0 & 0 & 0 & 0 \\ 0 & 0 & 0 & 0 & 0 & 0 \end{bmatrix}\right|_{\alpha_s} \tag{14a}$$

$$\mathbf{C}_i^{ae} = -\frac{1}{2}\rho U B l_{wi} \left.\begin{bmatrix} 0 & 0 & 0 & 0 & 0 & 0 \\ 0 & 2(D/B)C_D & (D/B)C'D - C_L & 0 & 0 & 0 \\ 0 & 2C_L & C_L' + (D/B)C_D & 0 & 0 & 0 \\ 0 & 2BC_M & BC_M' & 0 & 0 & 0 \\ 0 & 0 & 0 & 0 & 0 & 0 \\ 0 & 0 & 0 & 0 & 0 & 0 \end{bmatrix}\right|_{\alpha_s} \tag{14b}$$

where l_{wi} is the length along which the wind forces acting on the structural element are lumped to the node i. The above definition of the UEL is presented with generality and it is readily applicable to any FE software. Further details on the specified implementation of this UEL to Abaqus are described in Appendix II. Using this methodology, the wind induced forces are applied to all the bridge elements, including the deck, the arch and the piers.

RESULTS AND DISCUSSION

The deck of the Wild bridge has been designed to support two road lanes and one sidewalk as shown in Fig. 8. With this design, the road axis is eccentric 0.35 m with respect to the bridge axis which implies that the vehicles run over the bridge with certain eccentricity. In the previous work (Nguyen et al. 2015), it's observed that the larger the vibration at the sidewalk is obtained when the passing vehicle is transversely closer to the sidewalk. Therefore, the load case in which the vehicle runs on the lane 1 with eccentricity of 1.4 m is selected for this study (see Fig. 8). To eliminate the possible effect generated due to the suddenly applied aerodynamic wind forces on the dynamic response of the vehicle and to study the possible effect generated during the time that the vehicle enters and leaves the bridge, the external platforms with roughness surface are considered at both abutments of the bridge in all calculations.

As mentioned in section 4, in order to study the influence of the crosswind different levels of the basic wind velocity are used. In fact, a range from 5.0 to 30.0 m/s in increment of 0.5 m/s has been considered. Furthermore, for each level of basic wind velocity, a range of vehicle velocities ranging from 60 to 120 km/h, in increments of 10 km/h, is considered to investigate the ride comfort and safety of the road vehicle. An extensive number of analyses are performed and the main obtained results are presented and discussed below.

Effects of crosswind on the bridge vibration

In order to assess effects of the turbulent crosswind on the bridge vibration, the time histories of vertical and lateral acceleration of all points along the sidewalk are recorded in all calculations. The maximum acceleration at each point is then determined. Fig. 9(a) shows the peak vertical acceleration along the sidewalk for different levels of the basic wind velocity when the vehicle crosses the bridge at $v = 100$ km/h. The result without crosswind is also included for comparison. It can be observed that for gentle crosswind ($U_b = 5$ m/s) the vibration of deck is similar to the case without crosswind. It can be due to that the aerodynamic wind forces are too low to produce any meaningful inertia effects, comparing with the forces generated by the passing vehicle. But, as the crosswind is stronger and more moderate, the vibration of deck is larger. Furthermore, it is seen that the zone of arch span is the one more affected by the crosswind as expected, since the wind velocity in this zone is higher. In fact, if the basic wind velocity is of 25.0 m/s, the maximum vertical acceleration obtained at point C_1 can be up to 10.5 times higher than the case without crosswind and 1.5 times higher than the maximum acceleration allowed ($a_{lim} = 0.5\sqrt{f_0} = 0.81$ m/s^2) by some codes (BS 5400-2:2006 2006; RPX-95 1995) for deck vibration. Moreover, from Fig. 9(a) the impact effect can be observed when the vehicle enters and leaves the bridge. Such peak acceleration at the deck nearby the abutments would far exceed the admissible limit in SLS of vibration (a_{lim}). The human response to vibration depends, of course, on the level or magnitude of vibration, but also depends on the other important factors such as frequency content of the vibration, exposure time, direction of application, etc. Further analysis have been done in order to evaluate the human comfort. The RMS acceleration in one-third octave frequency bands are obtained from the acceleration time histories. These RMS acceleration are then compared with the vertical base curve for acceptable human response under storm conditions proposed by Irwin (Irwin 1978). A representative result is shown in Fig. 9(b), in which the vertical RMS accelerations at the point C_1 are represented for different levels of the basic wind velocity. The result in Fig. 9(b) reaffirms the important influence of crosswind on the vertical vibration of this bridge and the need for considering the aerodynamic actions introduced by wind in the general vibration assessment of bridges. Additionally, it can be seen that the RMS accelerations will exceed the limit comfort curve considering the threshold for frequent events when the wind is strong (25.0 m/s), which means that the human, in this case, pedestrian users feel or sense discomfort due to the bridge vibration.

Respect to the lateral vibration of the bridge, the same results are represented in Fig. 10. The peak lateral accelerations along the sidewalk are obtained and plotted for different levels of the basic wind velocity (U_b), and compared with the limit of comfort established by IAP-11 (IAP-11 2011) ($a_{lim} = 0.8$ m/s^2) (see Fig. 10(a)). The RMS accelerations in one-third octave frequency bands at the point C$_1$ are also plotted and compared with the lateral acceleration base curve for acceptable human response proposed by Irwin (Irwin 1978). Figure 10(a) shows that the peak lateral acceleration on the deck is only increased by the crosswind on the sections corresponding to the arch due to the increased transverse flexibility of the bridge in this area. Furthermore, this effect is only appreciable for relatively strong wind speeds, which is attributed to important slenderness of the deck and the reduced aerodynamic forces. However, from Fig. 10(b) it can be noted that the crosswind has an important effect on the frequency content of the acceleration signals of this structure, specially in the range $[0.4-10]$ Hz. The RMS acceleration in one-third octave bands at point C$_1$ increases with the wind velocity, and it nearly reaches the limit curve for $U_b = 25.0$ m/s. This demonstrates that, as expected, the pedestrians comfort decreased by increasing the lateral wind speed and it can only be tackled by using criteria that account for the excitation frequency, such as Iwin's

In order to explore the participation of the wind- and traffic-induced vibration on the frequency content of the response of the deck, the time histories of the deck acceleration is analyzed in the frequency domain. Fig. 11 shows the frequency content of the vertical and lateral acceleration at point C$_1$ when the vehicle crosses over the bridge at $V = 100$ km/h, for different basic wind speeds. It can be observed from Fig. 11(a) that three modes dominate the vertical deck vibration. The dominance of the first vertical mode is observed, specially for strong winds ($U_b = 25.0$ m/s), but it is also apparent the important participation of the third vertical mode (approximately 5 Hz) and the torsional mode (in the range of 10

Hz). This result directly questions the applicability of extended comfort criteria that are based on the assumption that the structure is completely dominated by a fundamental mode of vibration (BS 5400-2:2006 2006; RPX-95 1995). In comparison to the vertical vibration of the deck, the lateral vibration (Fig. 11(b)) is more dominated by the first lateral mode for wind velocities below 20 m/s, beyond this value a group of closely spaced high-order mode between 5 and 10 Hz increases significantly the response as shown in Fig. 11(b).

Effects of crosswind on the road vehicle vibration

In this section, the ride comfort and safety of road vehicle are addressed through the accelerations at the driver seat (see Fig. 3), the contact forces between the tire and road. The weighted RMS acceleration and the RMS acceleration in one-third octave frequency bands are obtained from the time histories of the vertical and lateral acceleration at the driver's seat in order to evaluate the vehicle users' comfort. The resulting accelerations are compared with the indicative ranges of comfort given by ISO 2631 (ISO 2631-1:1997 1997) and fatigue-decreased proficiency boundaries proposed by ISO 2631 (ISO 2631:1978 1978), respectively. Figure 12 shows the results for the vertical vibration of the vehicle. It can be observed that the maximum acceleration at driver's seat is hardly affected by crosswinds below ranging from 5 to 20 m/s (see Fig. 12(a)), which is also noticed for the the weighted RMS accelerations (see Fig. 12(b)). Furthermore, there are high increments of acceleration for strong wind ($U_b = 25.0$ m/s) compared with the other lower wind velocities. This is due to the fact that the strong wind increases the vehicle vibration on the one hand, and increases the bridge vibration on the other which also influences the vehicle vibration, as shown in Fig. 14(a). Interestingly, all recorded values of RMS accelerations in the vehicle are regarded as "uncomfortable" according to ISO's criterion (ISO

2631-1:1997 1997), including the case in which the wind is not considered and for all the vehicle velocities considered. The validity of the comfort criteria for the vertical vibrations in the vehicle considered should be questioned based on these results. Firstly, it is noted that the scope of this work is the global assessment of the user's comfort and safety due to the wind-vehicle-bridge interaction, and no attempt was made to simulate the filtering effect of the vehicle seat or other local effects in the vehicle. Secondly, the indicative comfort range proposed by ISO 2631 (ISO 2631-1:1997 1997) gives approximate indications of likely reactions to various magnitudes of overall vibration total values in public transport, and ISO 2631 does not define any limit for acceptable values of magnitude for comfort. From Fig. 12(c) and 12(d), it can be seen that the crosswind hardly effect on the vertical ride comfort of vehicle.

Fig. 13 shows the results of the lateral vibration of vehicle. It is observed that the crosswind influences significantly the lateral acceleration in the vehicle and the comfort of its user regarding vibrations in this direction. Indeed, the peak acceleration and the weighted RMS acceleration increase by increasing the crosswind velocity. The RMS accelerations in the one-third octave bands are also larger when the crosswind speed increases. The RMS accelerations almost reach the limit curve for fatigue-decreased proficiency when the velocity of the vehicle is 120 km/h and the crosswind speed is 25.0 m/s, indicating that the driver could feel fatigue and decrease his proficiency to drive. In contrast to the vertical vibration of the vehicle, its lateral vibration is not influenced by the bridge vibration, but is only influenced by its lateral vibration modes, as shown in Fig. 14(b).

Vehicle accidents can be categorized in three main types: overturning, side-slipping and yawing (rotational) accidents (Baker and Reynolds 1992). Side-slipping accidents and yawing may occur if the coefficient of friction between the tires and the road surface is low (Snæ björnsson et al. 2007; Zhou and Chen 2015) (e.g. in wet pavements). However, the assessment of side-slipping and, especially, yawing accidents, requires detailed information about the contact between the tires and the pavement, as well as the model of the driver's response (Chen and Cai 2004). This work will focus only on vehicle overturnings because it represents the most common type of wind-induced vehicle accidents (Baker and Reynolds 1992). It should be noted, however, that the methodology presented in this paper is applicable to the study of the other types of accidents.

An overturning accident occurs when one of the tire reactions is zero, in other words, the vertical load is transferred from the tires on the windward side of the vehicle to those on the leeward side. The Load Transfer Ratio (LTR) is employed to quantify the load transference and is defined as:

$$LTR = \frac{F_L - F_R}{F_L + F_R} \tag{15}$$

where F_L and F_R are the vertical tire reactions on the left (leeward) and right (windward) sides, respectively. The LTR is 0.0 when the loads on two sides are equal and ± 1.0 when all the load is transferred to the leeward side and the vehicle is on the verge of an overturning accident. The LTR of the front and rear wheels are plotted in Fig. 15(a) for a certain vehicle and wind velocity. It can be observed that the load transfer reaches larger value when the vehicle is at the arch span, as expected. This is because that the crosswind velocity in this section of the bridge is higher than those of other sections of the bridge. The LTR at the rear wheel is higher than at the front wheel, as expected. It is due to that the rear wheels have less gravity load from the carbody by the position of gravity centre, and therefore these wheels govern the overturning accident.

Based on the LTR, the critical wind speed can be determined for each vehicle velocity when at this speed the vehicle overturns. Consequently, the critical wind curve (CWC) can be obtained from the all critical wind speed for the whole range of the vehicle velocities. Figure 15(b) represents the CWC obtained in this work for the bridge. Assuming a vehicle velocity limit of 120 km/h, it is observed that no restriction should be imposed when the wind speed is below 15 m/s, which could be considered as the critical wind speed for this bridge.

CONCLUSIONS

In this paper, the dynamic effects of turbulent crosswind on the serviceability state of vibrations and the vehicle accident risk are addressed in a slender arch by means of the wind-vehicle-bridge interaction analyses. A new finite element is developed for the application of aerodynamic wind actions in general Finite Element Analysis software packages. This element is able to provide the aeroelastic wind forces. The results of the fully coupled nonlinear dynamic analysis drawn the following conclusions on the dynamic response of the studied bridge:

- The bridge vibration is significantly affected by the crosswind in terms of the peak acceleration and the frequency content when the crosswind is moderate and strong ($U_b > 15$ m/s). However, for lower wind speeds (below 10 m/S) the deck vibration is governed by the passing vehicle.

- The criteria for the SLS of vertical vibration based on the peak acceleration is easily exceeded at almost point of the deck when the crosswind is strong ($U_b = 25.0$ m/s). Analyzing in the frequency domain the vibration level is still below the limit comfort curve, and therefore, is comfortable. Furthermore, the vertical bridge vibration is significantly influenced by high-order vibration modes between 5 and 10 Hz that would be ignored according to code-based comfort criteria such as (BS 5400-2:2006 2006; RPX-95 1995).

- Previous research works observed the importance of the road roughness surface on the ride comfort of the vehicle. In this study, it is observed that it also depends on the vehicle velocity and the crosswind speed. It is observed that the crosswind has more effect on ride comfort of the vehicle in lateral direction than in the vertical direction. When the vehicle runs over the bridge with the velocity of 120 km/s and with a strong crosswind velocity ($U_b = 25.0$ m/s), the driver could experience the fatigue and decrease his proficiency to drive.
- For the "good" road surface quality considered in this study, the basic wind speed of 15 m/s could be considered as the critical speed in the studied bridge for the circulation.

ACKNOWLEDGEMENTS

The authors thank to other members of the team of Intitut für Betonbau at Technical University of Graz: Berhard Freytag, Michael Reichel, who provided the necessary information of the Wild bridge design. K.Nguyen and O. Rio also thank to the MINECO of Spain for the support of the project BIA2013-48480-C2-1R.

REFERENCES

American Association of State Highway and Transportation Officials (1998). *AASHTO LRFD: Bridge design specifications*. Washington, EE UU.

Azizinamini, A., Barth, K., Dexter, R., and Rubeiz, C. (2004). "High Performance Steel: Research FrontHistorical Account of Research Activities." *Journal of Bridge Engineering*, 9(3), 212–217.

Baker, C. J. and Reynolds, S. (1992). "Wind-induced accidents of road vehicles." *Accident Analysis and Prevention*, 24(6), 559–575.

Boggs, D. and Petersen, C. P. (1995). "Acceleration indexes for human comfort in tall buildings - peak or rms?

BS 5400-2:2006 (2006). *Steel, concrete and composite bridges - Part 2: Specification for loads*. British Standard, UK.

BS 6841:1987 (2012). *Guide to measurement and evaluation of human exposure to whole-body mechanical vibration and repeated shock*.

Cai, C. and Chen, S. (2004). "Framework of vehiclebridgewind dynamic analysis." *Journal of Wind Engineering and Industrial Aerodynamics*, 92(7-8), 579–607.

Camara, A., Nguyen, K., Ruiz-Teran, A., and Stafford, P. (2014). "Serviceability limit state of vibrations in under-deck cable-stayed bridges accounting for vehicle-structure interaction." *Engineering Structures*, 61, 61–72.

CEN (2005a). *EN 1337-3:2005 Structural bearings. Part 3: Elastomeric bearings.* rue de Stassart, 36B-1050 Brussels.

CEN (2005b). *EN 1991-1-4: Actions on structures - Part 1-4: General actions - Wind actions*. rue de Stassart, 36B-1050 Brussels.

Chen, S. R. and Cai, C. S. (2004). "Accident assessment of vehicles on long-span bridges in windy environments." *Journal of Wind Engineering and Industrial Aerodynamics*, 92(12), 991–1024.

Chen, X., Matsumoto, M., and Kareem, A. (2000). "Time Domain Flutter and Buffeting Response Analysis of Bridges." *Journal of Engineering Mechanics*, 126(1), 7–16.

Davenport, A. (1962). "Buffeting of a Suspension Bridge by Storm Winds." *Journal of the Structural Division*, 88(3), 233–270.

Dodds, C. and Robson, J. (1973). "The description of road surface roughness." *Journal of Sound and Vibration*, 31(2), 175–183.

Griffin, M. J. (1990). *Handbook of Human Vibration*. Academic Press Inc. (London) Limited.

Guo, W. H. and Xu, Y. L. (2006). "Safety Analysis of Moving Road Vehicles on a Long Bridge under Crosswind." *Journal of Engineering Mechanics*, 132(4), 438–446.

Hilber, H. M., Hughes, T. J., and Taylor, R. L. (1977). "Improved numerical dissipation for time integration algorithms in structural dynamics." *Earthquake Engineering and Structural Dynamics*, 5, 283–292.

IAP-11 (2011). *IAP-11: Instrucción sobre las acciones a considerar en el proyecto de puentes de carretera (in Spanish)*.

Irwin, A. W. (1978). "Human response to dynamic motion of structures." *The Structural Engineer*, 56A(9), 237–244.

ISO 2631-1:1997 (1997). *Mechanical vibration and shock – Evaluation of human exposure to whole-body vibration – Part 1: General requirements*. International Organization for Standardization, Gineva.

ISO 2631:1978 (1978). *Guide for the evaluation of human exposure to whole-body vibration*. International Organization for Standardization, Gineva.

ISO 8608:1995 (1995). *Mechanical vibration - Road surface profiles - Reporting of measured data*. International Organization for Standardization (ISO), Gineva.

JCSS (2001a). *Probabilistic Model Code - Part 2: Load Models*.

JCSS (2001b). *Probabilistic Model Code - Part 3: Material Properties*.

Kamash, K. M. A. and Robson, J. D. (1978). "The Application of Isotropy in Road Surface Modelling." *Journal of Sound and Vibration*, 57(1), 89–100.

Kühne, M. and Orgass, M. (2009). "Prüfbericht PB 1.1/09-126-4 : Überwachung und Prüfung von UHFRC für das Bauvorhaben, Wild-Brücke." *Report no.*, MFPA Leipzig GmbH.

Miyata, T. and Yamada, H. (1990). "Coupled flutter estimate of a suspension bridge." *Journal of Wind Engineering and Industrial Aerodynamics*, 33, 341–348.

Moghimi, H. and Ronagh, H. R. (2008). "Development of a numerical model for bridgevehicle interaction and human response to traffic-induced vibration." *Engineering Structures*, 30(12), 3808–3819.

Nguyen, K., Freytag, B., Ralbovsky, M., and Rio, O. (2015). "Assessment of serviceability limit state of vibrations in the UHPFRC-Wild bridge through an updated FEM using vehicle-bridge interaction." *Computers & Structures*, 156, 29–41.

Roeder, C. W., Barth, K. E., and Bergman, A. (2004). "Effect of Live-Load Deflections on Steel Bridge Performance." *Journal of Bridge Engineering*, 9(3), 259–267.

RPX-95 (1995). *RPX-95: Recommendations for the project of composite road bridges (in Spanish)*. Spain.

Sayers, M. W. (1988). "Dynamic Terrain Inputs to Predict Structural Integrity of Ground Vehicles." *Report No. UMTRI-88-16*, University of Michigan, Transportation Research Institute, Michigan.

Scanlan, R. (1978). "The action of flexible bridges under wind, II: Buffeting theory." *Journal of Sound and Vibration*, 60(2), 201–211.

Scanlan, R. and Tomko, A. (1971). "Airfoil and Bridge Deck Flutter Derivatives." *Journal of the Engineering Mechanics Division*, 97(6), 1717–1737.

SIMULIA (2011). *Abaqus Analysis User's Manual, v6.11*. Dassalt Systemes SIMULIA Corp.

Snæ björnsson, J. T., Baker, C. J., and Sigbjörnsson, R. (2007). "Probabilistic assessment of road vehicle safety in windy environments." *Journal of Wind Engineering and Industrial Aerodynamics*, 95(9-11), 1445–1462.

Sparowitz, L., Freytag, B., Reichel, M., and Zimmermann, W. (2011). "Wild Bridge - A Sustainable Arch Made of UHPFRC." *3rd Chinese - Croatian Joint Colloquium: Sustainable Arch Bridges*, Zagreb, Croatia, 45–70.

Sterling, M., Quinn, A. D., Hargreaves, D. M., Cheli, F., Sabbioni, E., Tomasini, G., Delaunay, D., Baker, C. J., and Morvan, H. (2010). “A comparison of different methods to evaluate the wind induced forces on a high sided lorry.” *Journal of Wind Engineering and Industrial Aerodynamics*, 98(1), 10–20.

Strømmen, E. (2006). *Theory of Bridge Aerodynamics*. Springer.

Veers, P. S. (1988). “Three-dimensional wind simulation.” *SANDIA report, SAND88-0152 UC-261*, Sandia National Laboratories, California, USA.

Weller, H. G., Tabor, G., Jasak, H., and Fureby, C. (1998). “A tensorial approach to computational continuum mechanics using object-oriented techniques.” *Computers in Physics*, 12(6), 620–631.

Wright, R. N. and Walker, W. H. (2004). “Criteria for deflection of steel bridges.” *Bulletin for the America Iron and Steel Institute*, 19.

Xu, Y. and Guo, W. (2004). “Effects of bridge motion and crosswind on ride comfort of road vehicles.” *Journal of Wind Engineering and Industrial Aerodynamics*, 92(7-8), 641–662.

Xu, Y. L. and Guo, W. H. (2003). “Dynamic analysis of coupled road vehicle and cable-stayed bridge systems under turbulent wind.” *Engineering Structures*, 25, 473–486.

Xu, Y. L., Sun, D. K., Ko, J. M., and Lin, J. H. (2000). “Fully coupled buffeting analysis of Tsing Ma suspension bridge.” *Journal of Wind Engineering and Industrial Aerodynamics*, 85(1), 97–117.

Zhou, Y. and Chen, S. (2015). “Fully coupled driving safety analysis of moving traffic on long-span bridges subjected to crosswind.” *Journal of Wind Engineering and Industrial Aerodynamics*, 143, 1–18.

APPENDIX I. PROPERTIES OF THE HIGH-SIDED TRUCK

The main properties of the high-sided truck are listed in Table III.

APPENDIX II. IMPLEMENTATION OF USER ELEMENT

The user element is composed by 2 nodes. Each node has six degrees of freedom. In order to implement this element into the Abaqus software, there are two essential outputs that are required to be updated in the UEL subroutine (SIMULIA 2011). In particular, the residual quantity $\mathbf{RHS} := \mathbf{F}$ and the element Jacobian $\mathbf{AMATRX} := -\partial\mathbf{F}/\partial\mathbf{u}$ must be updated in every interaction. The program Abaqus uses an implicit time integration and a full Newton solution technique to solve the static and dynamic problem. In the static analysis, the user element implemented here does not contribute any stiffness to the model, while this element will provide the nodal forces to the model in the dynamic analysis. The nodal forces depend on the values of the degrees of freedom of the nodes and according to (13) the nodal forces provided by the element is expressed as

$$\mathbf{G} = \mathbf{C}\dot{\mathbf{u}} + \mathbf{K}\mathbf{u} \tag{16}$$

where

$$\mathbf{C} = \begin{bmatrix} \mathbf{C}_i^{ae} & \mathbf{0} \\ \mathbf{0} & \mathbf{C}_i^{ae} \end{bmatrix} \text{ and } \mathbf{K} = \begin{bmatrix} \mathbf{K}_i^{ae} & \mathbf{0} \\ \mathbf{0} & \mathbf{K}_i^{ae} \end{bmatrix} \tag{17}$$

According to (SIMULIA 2011), for the integration dynamic analysis the residual quantity and the element Jacobian at time $t+\Delta t$ must be determined as following

$$\mathbf{RHS} = \mathbf{F} = -\mathbf{M}\ddot{\mathbf{u}}_{t+\Delta t} + (1+\alpha)\mathbf{G}_{t+\Delta t} - \alpha\mathbf{G}_t \tag{18a}$$

$$\mathbf{AMATRX} = \mathbf{M}(\mathrm{d}\ddot{\mathbf{u}}/\mathrm{d}\mathbf{u}) + (1+\alpha)\mathbf{C}(\mathrm{d}\dot{\mathbf{u}}/\mathrm{d}\mathbf{u}) + (1+\alpha)\mathbf{K} \tag{18b}$$

where $\mathbf{M}^{NM}$ is the mass matrix of the user element (for the implemented element, $\mathbf{M}^{NM} = [\mathbf{0}]$), α is the factor for numerical damping used in HHT method. The values of the nodal forces are recorded as solution-dependent state variables for each time increment in order to determine **RHS** as defined in equation (18a).

APPENDIX III. AERODYNAMIC PROPERTIES OF BRIDGE

The aerodynamic coefficients and their derivatives are obtained from two dimensional Computational Fluid Dynamic analysis of the deck, arch and pier sections using OpenFOAM v.2.3 (Weller et al. 1998). The turbulence model follows the Reynolds Average Simulation (RAS) technique. The Reynolds number in the analyses is in the order of 10^7. Care was taken on the selection of the mesh size. After a sensitivity analysis the element size in the vicinity of the obstacles is selected as 3 mm.

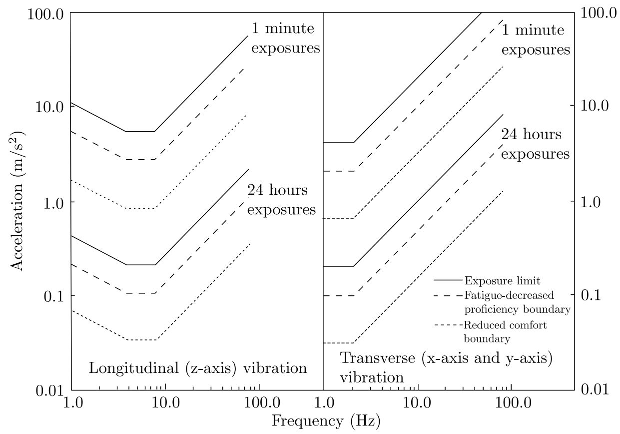

FIG. 1. Exposure limits, fatigue-decreased proficiency boundaries and reduced comfort boundaries to whole-body vibrations given in ISO 2631:1978 (adapted from Handbook of Human Vibration, M. J. Griffin (Griffin 1990), Chapter 10 “Whole-body Vibration Standards”, 415–451, Copyright 1990, with permission from Elsevier)

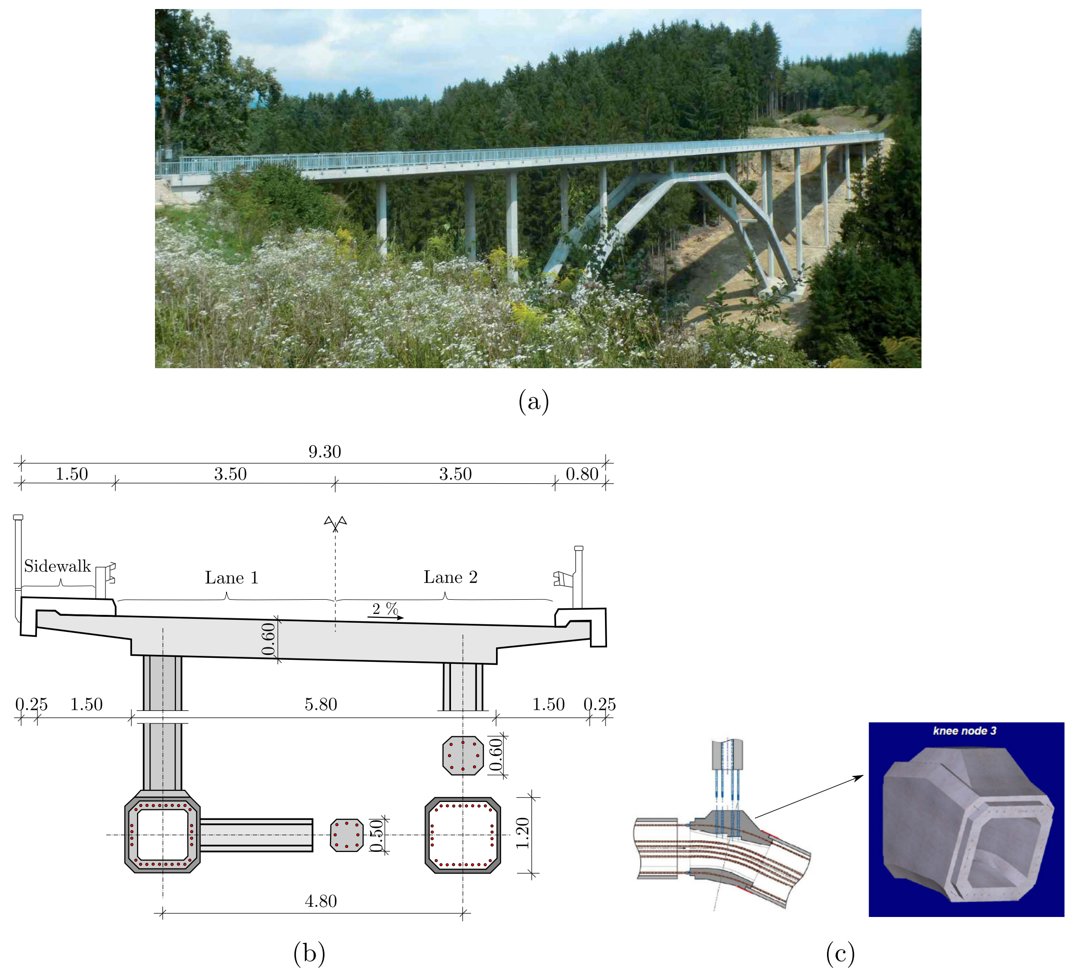

FIG. 2. Wild Bridge: (a) general view (image by L. Sparowitz), (b) cross section, (c) knee node

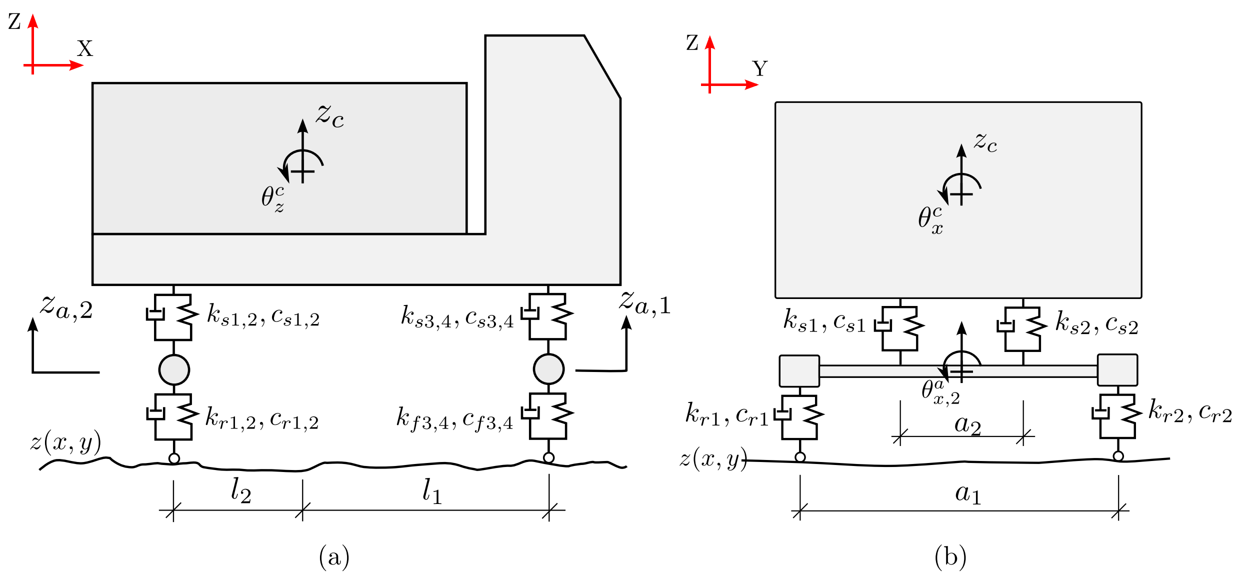

FIG. 3. High-sided vehicle model in dynamic analysis: (a) side view, (b) front view

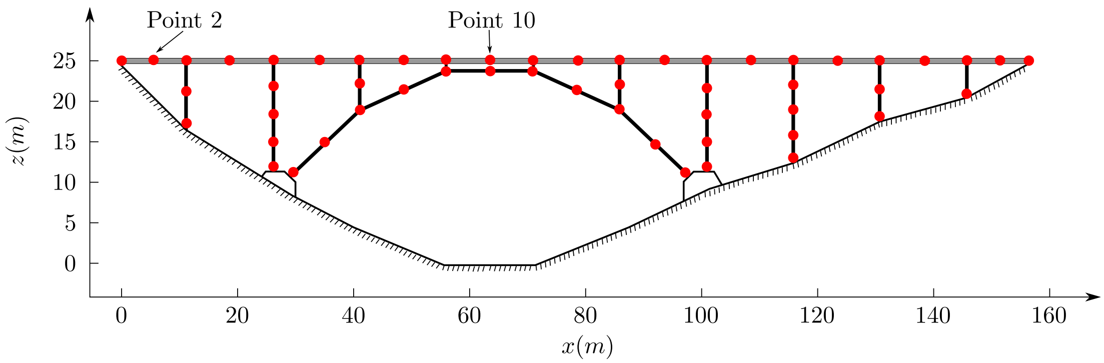

(a)

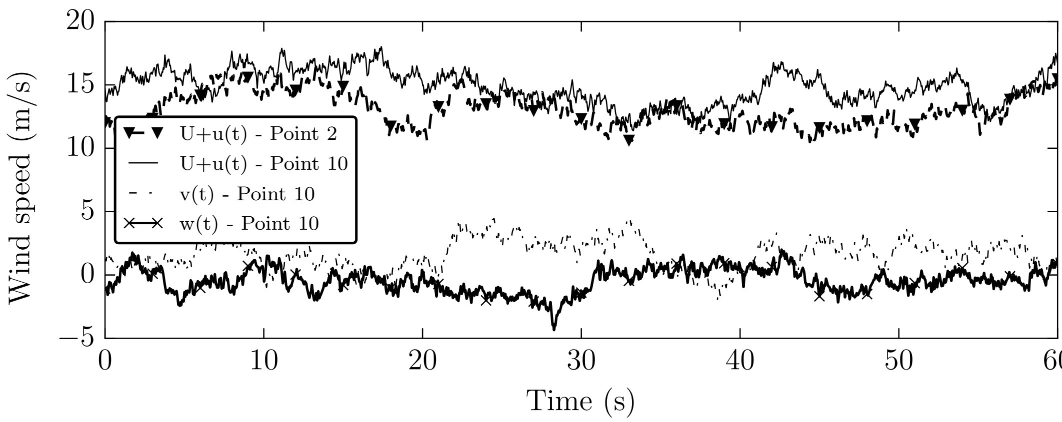

(b)

FIG. 4. Simulated wind speed: (a) Position of 53 points for wind speed time histories, (b) Turbulent wind speed at different points for $U_b = 10.0$ m/s

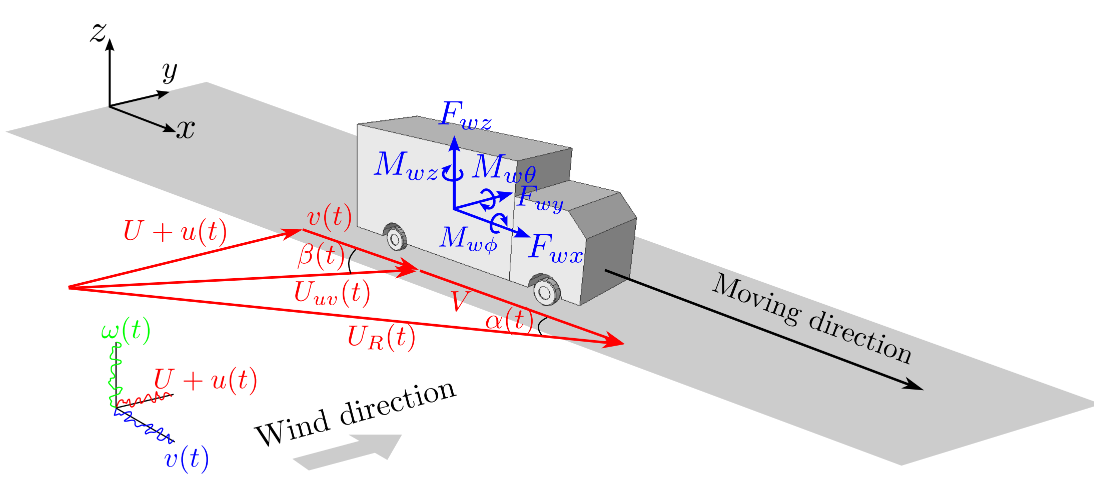

FIG. 5. Relative wind velocity to the running vehicle

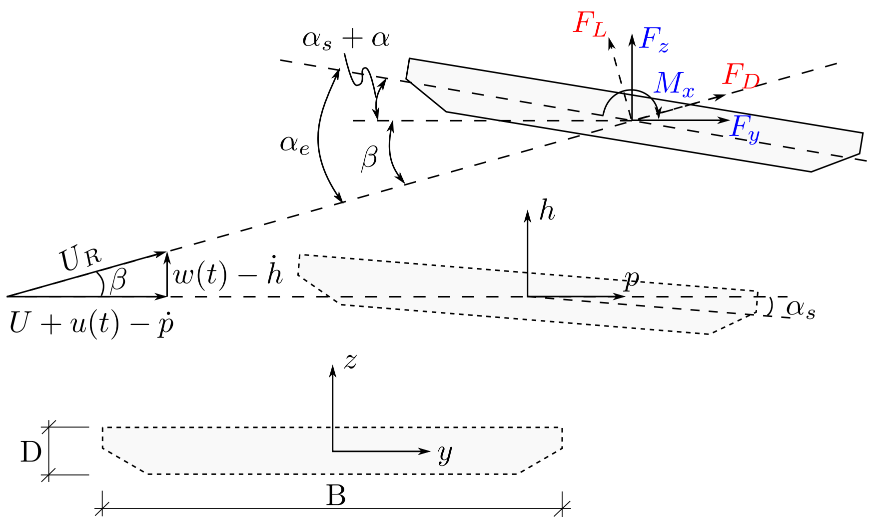

FIG. 6. Diagram of turbulent crosswind actuating on bridge elements

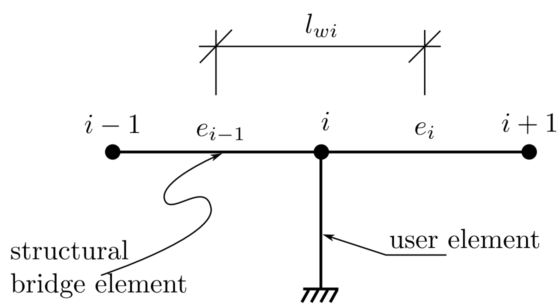

FIG. 7. User element for modelling the aeroelastic wind forces

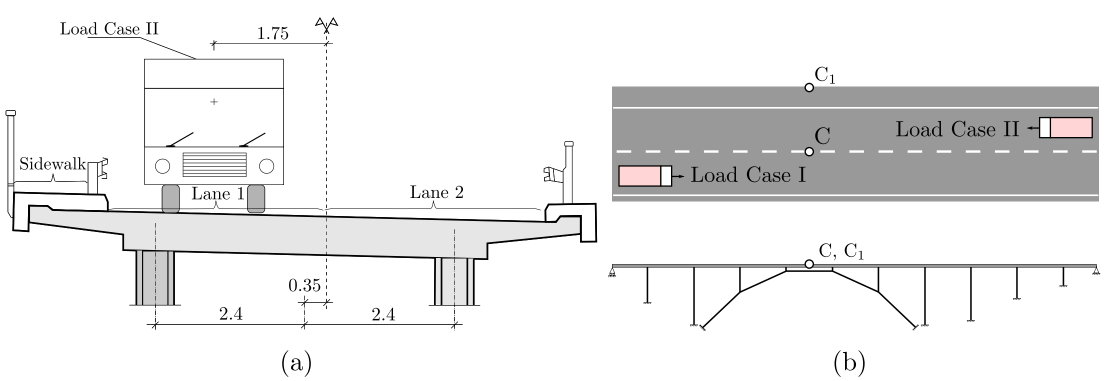

FIG. 8. Load case considered in this study: (a) cross section, (b) plan view and elevation of the bridge, including some control points employed to refer the ongoing results

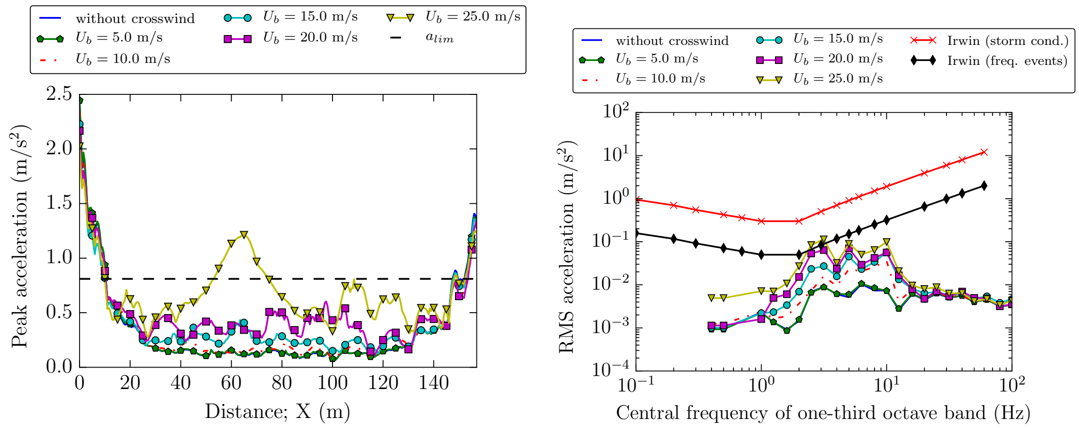

(a) (b)

FIG. 9. Effects of crosswind on the vertical vibration of the bridge at v=100 km/h: (a) Peak acceleration along sidewalk, (b) RMS acceleration in one-third octave frequency bands at point C$_1$

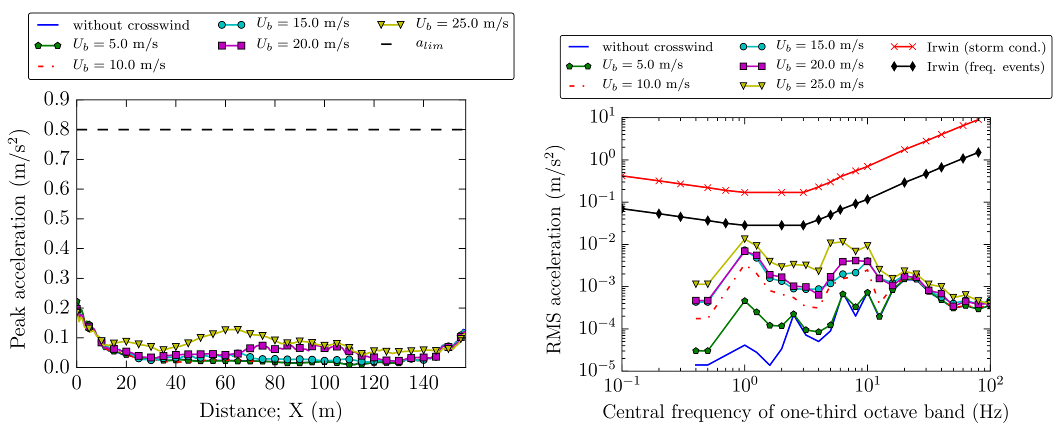

(a) (b)

FIG. 10. Effects of crosswind on the lateral vibration of the bridge at v=100 km/h: (a) Peak acceleration along sidewalk, (b) RMS acceleration in one-third octave frequency bands at point C$_1$.

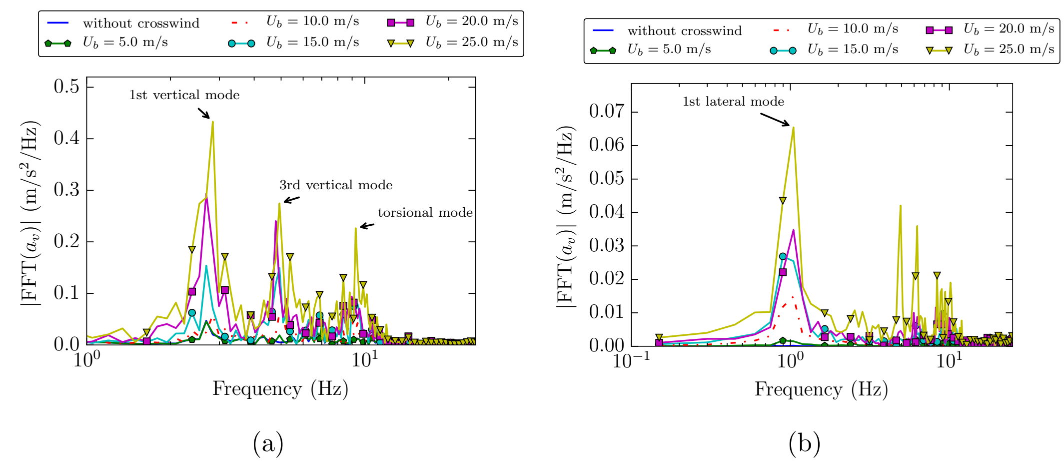

FIG. 11. Frequency content of deck acceleration at point C_1 when the vehicle runs over the bridge at $V = 100$ km/h: (a) vertical acceleration, (b) lateral acceleration.

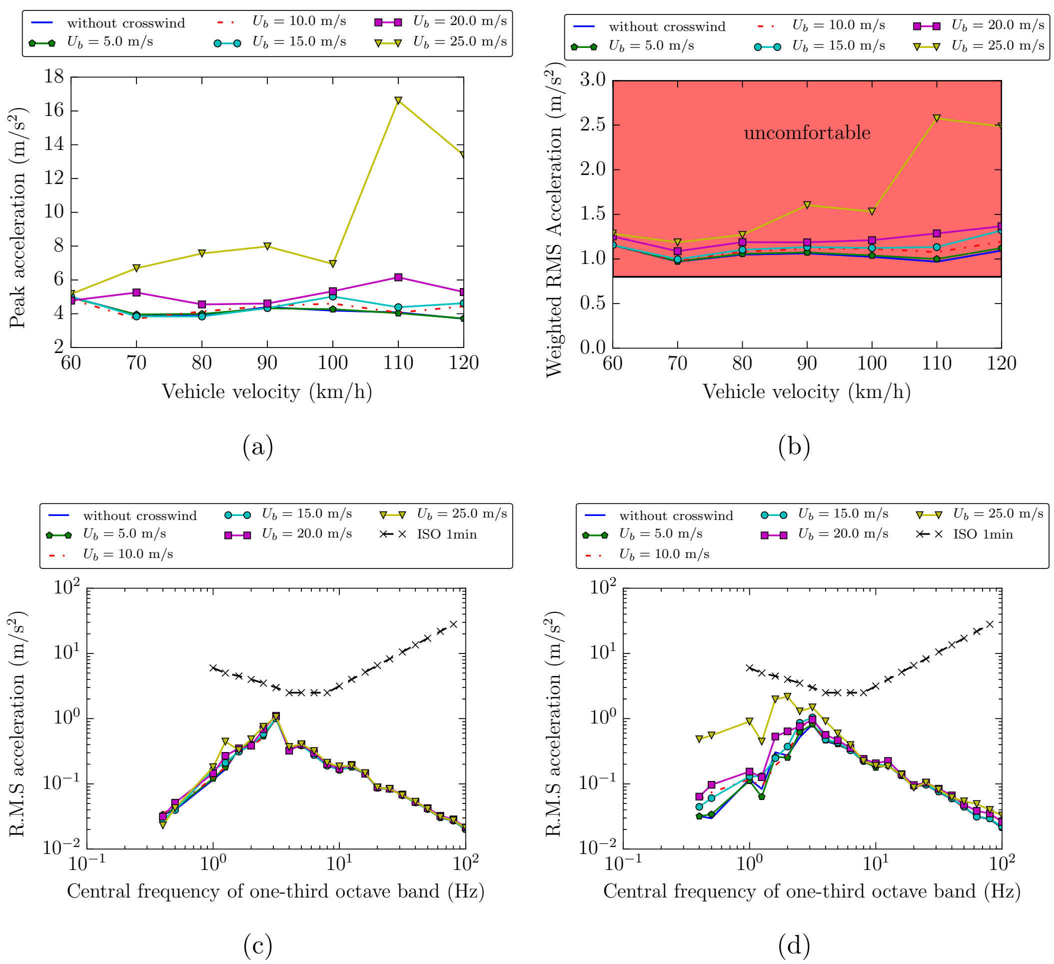

FIG. 12. Vertical vibration of the vehicle: (a) Peak acceleration, (b) Weighted RMS acceleration, (c) Fatigue curve for $V = 60$ km/h, (d) Fatigue curve for $V = 120$ km/h

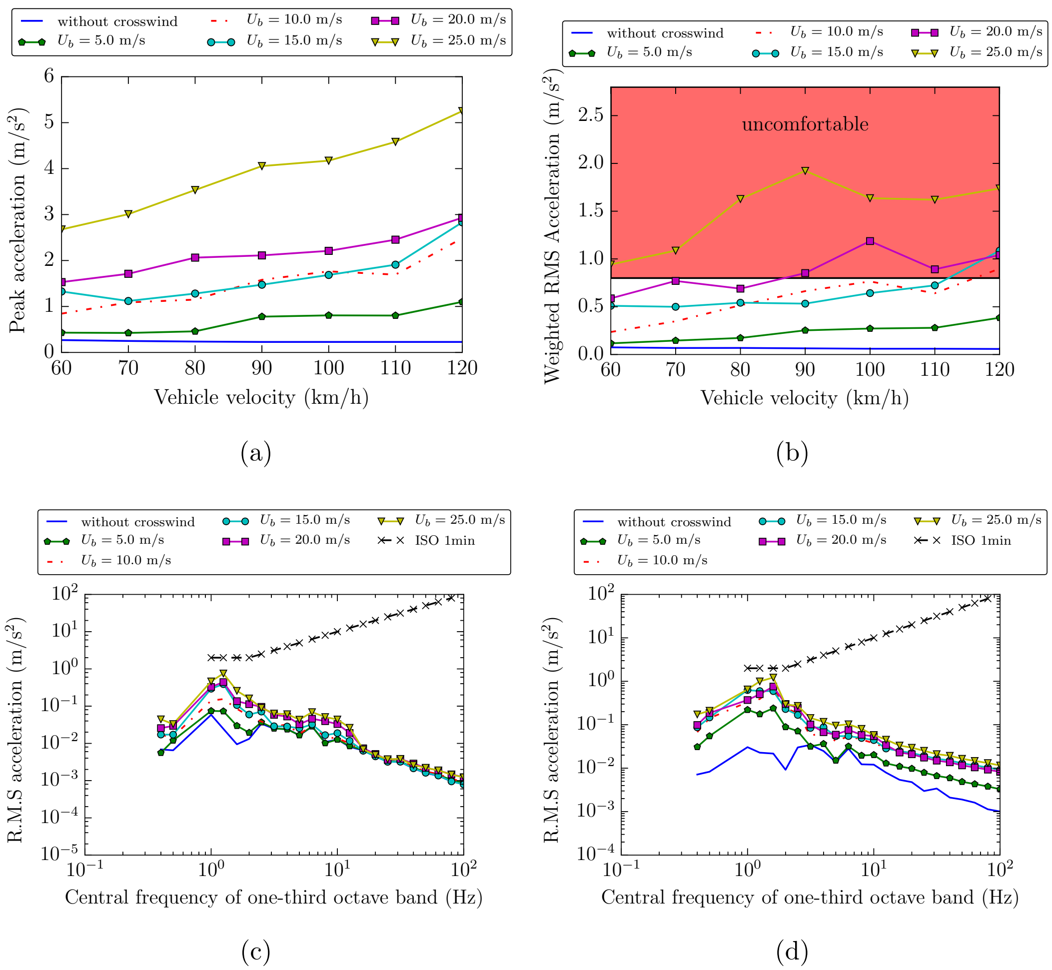

FIG. 13. Lateral vibration of the vehicle: (a) Peak acceleration, (b) Weighted RMS acceleration, (c) Fatigue curve for $V = 60$ km/h, (d) Fatigue curve for $V = 120$ km/h

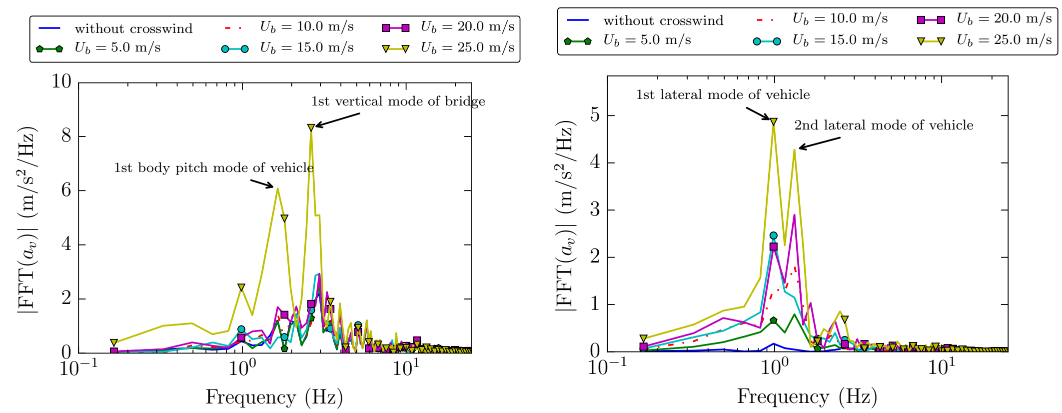

(a) (b)

FIG. 14. Frequency content of the acceleration at driver's seat when the vehicle runs over the bridge at $V = 110$ km/h: (a) vertical acceleration, (b) lateral acceleration.

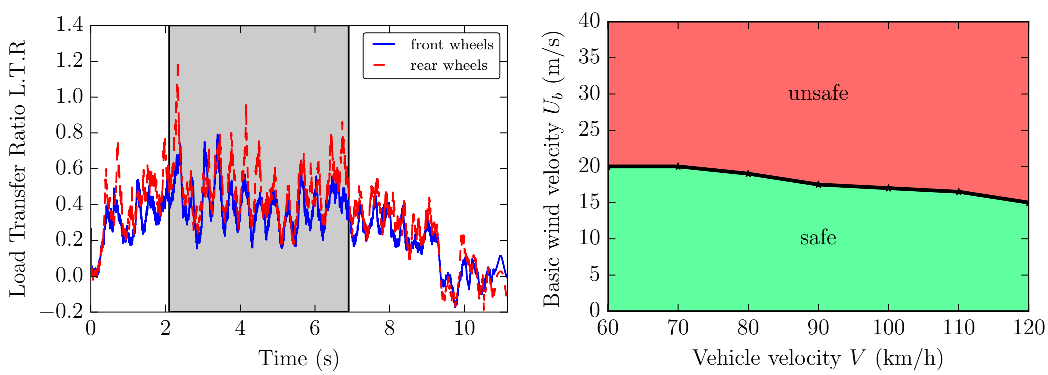

(a) (b)

FIG. 15. Vehicle overturning accident assessment: (a) Load Transfer Ratio for $U_b = 20.0$ m/s and $V = 60$ km/h, (b) Critical Wind Curve

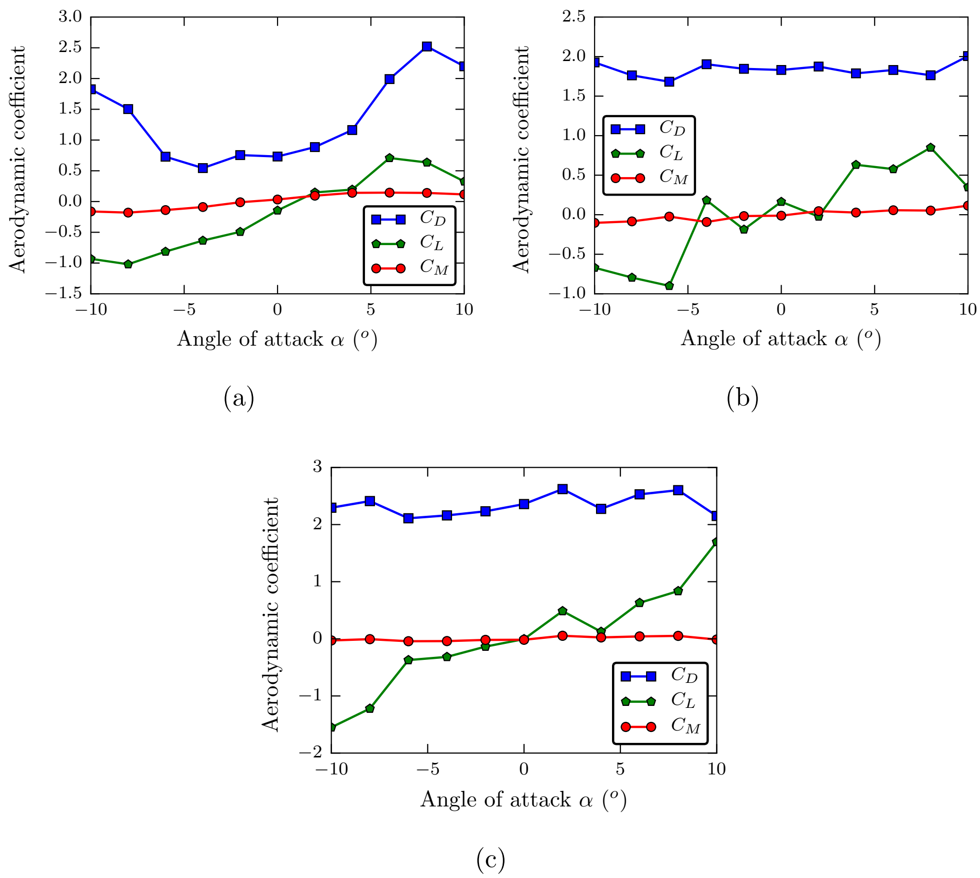

FIG. 16. Aerodynamic coefficients of bridge elements: (a) deck, (b) arch, (c) pier

TABLE 1. Main characterization of parameters of the numerical model of Wild bride

Notation	Parameter	Unit	Adopted and/or updated value	References
E_a	Elastic modulus of arches	GPa	53.3	(Nguyen et al. 2015)
ρ_a	Mass density of arches	kg/m^3	2590	(JCSS 2001a; Kühne and Orgass 2009)
E_p	Elastic modulus of bridge piers	GPa	41.4	(Nguyen et al. 2015)
ρ_p	Mass density of bridge piers	kg/m^3	2500	(JCSS 2001a)
E_d	Elastic modulus of deck	GPa	38.0	(Nguyen et al. 2015)
ρ_d	Mass density of deck	kg/m^3	2518.7	(Nguyen et al. 2015)
m_d	Nonstructural mass on deck	kg/m^2	216.0	(JCSS 2001a)
h_d	Thickness of deck	m	0.601	(Nguyen et al. 2015)
E_{eb}	Bulk modulus of the bearing	GPa	834	(JCSS 2001b)

TABLE 2. Summary of first six modes of vibration of the bridge

Mode	Frequency (Hz)	Description
1	0.874	1st lateral bending
2	2.371	2nd lateral bending
3	2.586	1st vertical bending
4	2.895	2nd vertical bending
5	3.971	3rd vertical bending
6	4.607	3rd lateral bending

TABLE 3. Main parameters of the high-sided truck

Notation	Parameter	Value
m_c	Mass of truck body (kg)	4480
J_{cy}	Pitching moment of inertia of track body (kg.m^2)	5516
J_{cx}	Rolling moment of inertia of track body (kg.m^2)	1349
J_{cz}	Yawing moment of inertia of track body (kg.m^2)	100000
$m_{r,i}$ $(i = 1, 2)$	Mass of rear axle set(kg)	710
$m_{f,i}$ $(i = 1, 2)$	Mass of front axle set(kg)	800
$k_{z,si}$ $(i = 1, 2, 3, 4)$	Vertical stiffness of suspension along Z axis (kN/m)	399
$k_{y,si}$ $(i = 1, 2, 3, 4)$	Lateral stiffness of suspension along Z axis (kN/m)	299
$c_{z,si}$ $(i = 1, 2)$	Vertical damping of rear suspension along Z axis (kN s/m)	5.18
$c_{y,si}$ $(i = 1, 2)$	Lateral damping of rear suspension along Z axis (kN s/m)	5.18
$c_{z,si}$ $(i = 3, 4)$	Vertical damping of front suspension along Z axis (kN s/m)	23.21
$c_{y,si}$ $(i = 3, 4)$	Lateral damping of front suspension along Z axis (kN s/m)	23.21
$k_{z,fi}$ $(i = 1, 2)$	Vertical stiffness of front tire (kN/m)	351
$k_{z,ri}$ $(i = 1, 2)$	Vertical stiffness of rear tire (kN/m)	351
$k_{y,fi}$ $(i = 1, 2)$	Lateral stiffness of front tire (kN/m)	121
$k_{y,ri}$ $(i = 1, 2)$	Lateral stiffness of rear tire (kN/m)	121
$c_{z,fi}$ $(i = 1, 2)$	Vertical damping of front tire (kN s/m)	0.80
$c_{z,ri}$ $(i = 1, 2)$	Vertical damping of rear tire (kN s/m)	0.80
$c_{y,fi}$ $(i = 1, 2)$	Lateral damping of front tire (kN s/m)	0.80
$c_{y,ri}$ $(i = 1, 2)$	Lateral damping of rear tire (kN s/m)	0.80
l_1	Distance (m)	3.0
l_2	Distance (m)	5.0
l_3	Distance (m)	2.7
b_1	Distance (m)	1.10
b_2	Distance (m)	0.80
h_2	Distance (m)	1.30
A_f	Reference area (m^2)	10.5
h_f	Reference height (m)	1.5

List of figure captions

- Figure 1: Exposure limits, fatigue-decreased proficiency boundaries and reduced comfort boundaries to whole-body vibrations given in ISO 2631:1978 (adapted from Handbook of Human Vibration, M. J. Griffin (Griffin 1990), Chapter 10 Whole-body Vibration Standards, 415–451, Copyright 1990, with permission from Elsevier)

- Figure 2: Wild Bridge: (a) general view (taken by L. Sparowitz), (b) cross section, (c) knee node
- Figure 3: High-sided vehicle model in dynamic analysis: (a) side view, (b) front view
- Figure 4: Simulated wind speed: (a) Position of 53 points for wind speed time histories, (b) Turbulent wind speed at different points for $U_b = 10.0$ m/s
- Figure 5: Relative wind velocity to the running vehicle
- Figure 6: Diagram of turbulent crosswind actuating on bridge elements
- Figure 7: User element for modelling the aeroelastic wind forces
- Figure 8: Load case considered in this study: (a) cross section, (b) plan view and elevation of the bridge, including some control points employed to refer the ongoing results
- Figure 9: Effects of crosswind on the vertical vibration of the bridge at v=100 km/h: (a) Peak acceleration along sidewalk, (b) RMS acceleration in one-third octave frequency bands at point C_1
- Figure 10: Effects of crosswind on the lateral vibration of the bridge at v=100 km/h: (a) Peak acceleration along sidewalk, (b) RMS acceleration in one-third octave frequency bands at point C_1
- Figure 11: Frequency content of deck acceleration at point C_1 when the vehicle runs over the bridge at $V = 100$ km/h: (a) vertical acceleration, (b) lateral acceleration

- Figure 12: Vertical vibration of the vehicle: (a) Peak acceleration, (b) Weighted RMS acceleration, (c) Fatigue curve for $V = 60$ km/h, (d) Fatigue curve for $V = 120$ km/h

- Figure 13: Lateral vibration of the vehicle: (a) Peak acceleration, (b) Weighted RMS acceleration, (c) Fatigue curve for $V = 60$ km/h, (d) Fatigue curve for $V = 120$ km/h

- Figure 14: Frequency content of the acceleration at driver's seat when the vehicle runs over the bridge at $V = 110$ km/h: (a) vertical acceleration, (b) lateral acceleration

- Figure 15: Vehicle overturning accident assessment: (a) Load Transfer Ratio for $U_b = 20.0$ m/s and $V = 60$ km/h, (b) Critical Wind Curve

- Figure 16: Aerodynamic coefficients of bridge elements: (a) deck, (b) arch, (c) pier